PNAS RESEARCH ARTICLE | NEUROSCIENCE

Fragile X mental retardation protein coordinates neuron-to-glia communication for clearance of developmentally transient brain neurons

Chunzhu Song[a] and Kendal Broadie[a,b,c,d,1]

Edited by Alex Kolodkin, Johns Hopkins University School of Medicine, Baltimore, MD; received October 5, 2022; accepted February 7, 2023

In the developmental remodeling of brain circuits, neurons are removed by glial phagocytosis to optimize adult behavior. Fragile X mental retardation protein (FMRP) regulates neuron-to-glia signaling to drive glial phagocytosis for targeted neuron pruning. We find that FMRP acts in a mothers against decapentaplegic (Mad)-insulin receptor (InR)-protein kinase B (Akt) pathway to regulate pretaporter (Prtp) and amyloid precursor protein-like (APPL) signals directing this glial clearance. Neuronal RNAi of *Drosophila fragile X mental retardation 1* (*dfmr1*) elevates *mad* transcript levels and increases pMad signaling. Neuronal *dfmr1* and *mad* RNAi both elevate phospho–protein kinase B (pAkt) and delay neuron removal but cause opposite effects on InR expression. Genetically correcting pAkt levels in the *mad* RNAi background restores normal remodeling. Consistently, neuronal *dfmr1* and *mad* RNAi both decrease Prtp levels, whereas neuronal *InR* and *akt* RNAi increase Prtp levels, indicating FMRP works with pMad and insulin signaling to tightly regulate Prtp signaling and thus control glial phagocytosis for correct circuit remodeling. Neuronal *dfmr1* and *mad* and *akt* RNAi all decrease APPL levels, with the pathway signaling higher glial endolysosome activity for phagocytosis. These findings reveal a FMRP-dependent control pathway for neuron-to-glia communication in neuronal pruning, identifying potential molecular mechanisms for devising fragile X syndrome treatments.

glia | phagocytosis | insulin | PDF-tri clock neurons | *Drosophila*

Significance

Brain circuits are remodeled by the removal of neurons via glial engulfment and phagocytosis. The mechanism requires neuron-to-glia signaling to identify the targeted neuron, recruit glia, and trigger phagocytosis. This normal optimization process goes awry in neurological disease states such as fragile X syndrome (FXS), a leading heritable cause of intellectual disability and autism spectrum disorders. Epigenetic silencing of the mRNA-binding translational regulator fragile X mental retardation protein (FMRP) elevates mothers against decapentaplegic (Mad) transcript levels to increase phospho-Mad (pMad) signaling and prevent brain circuit remodeling. In neurons, this FMRP-dependent regulatory network interacts with insulin receptor (InR) phospho–protein kinase B (pAkt) control of two neuron-to-glia signals driving phagocytosis. This mechanism is critical for normal and diseased brain circuit remodeling.

Neuron-to-glia communication has critical roles in controlling brain circuit remodeling (1–3). Neuronal signaling induces glial phagocytosis from synapses to whole neurons, crucial in normal brains and in neurodevelopmental disorder conditions (2, 4–6). Disruption of neuron-to-glia communication causes aberrant neuronal pruning, resulting in defects ranging from defective synaptic transmission (7, 8) to impaired circuit wiring (9) to transient neuroinflammation (10, 11). A key case is fragile X syndrome (FXS), a leading intellectual disability and autism spectrum disorder (12, 13), typically caused by the epigenetic loss of fragile X mental retardation protein (FMRP) owing to expanded CGG repeats in the 5′-untranslated region of *fragile X mental retardation 1* (*fmr1*) (13, 14). In neurons, FMRP binds to specific transcripts to regulate protein translation during brain circuit development and later plasticity, including synaptic connectivity remodeling (15) and intercellular signaling mechanisms (16, 17). In the *Drosophila* FXS disease model, FMRP loss blocks removal of the developmentally transient pigment-dispersing factor (PDF)-Tri peptidergic neurons from the juvenile brain (15). Cell-specific RNAi studies show that FMRP is required only in neurons, not glia, to transcellularly activate glial phagocytosis driving PDF-Tri neuron clearance (18). Thus, FMRP-dependent neuron-to-glia communication drives targeted neuron pruning, but the molecular mechanisms remain largely unknown.

FMRP regulates bone morphogenic protein (BMP) and insulin-like peptide (ILP) signaling (19). Activated *Drosophila* BMP receptors phosphorylate mothers against decapentaplegic (pMad) to control gene transcription, including the insulin receptor (InR) (20, 21). InRs phosphorylate protein kinase B (pAkt) (22, 23) to suppress dendrite pruning (22). Importantly, mouse FMRP binds *smad* messenger ribonucleic acid (mRNA) (*Drosophila mad* homologue) (23), and *Drosophila* FMRP regulates pMad signaling levels in neurons (24). Moreover, FMRP loss elevates InR-dependent signaling (25). In neuron-to-glia communication, pretaporter (Prtp) and amyloid precursor protein like (APPL) from neurons both activate glial phagocytosis (26, 27). *Drosophila* Prtp traffics to the neuron surface to bind the glial phagocytotic receptor draper (Drpr) (26, 28). Loss of neuronal FMRP decreases glial Drpr expression (18), consistent with FMRP-dependent Prtp signaling. *Drosophila* APPL has a cleavable N terminus, and APPL release from neurons

Author contributions: C.S. designed research; C.S. performed research; C.S. contributed new reagents/analytic tools; C.S. analyzed data; K.B. editing, funding; and C.S. and K.B. wrote the paper.

The authors declare no competing interest.

This article is a PNAS Direct Submission.

[1]To whom correspondence may be addressed. Email: kendal.broadie@vanderbilt.edu.

This article contains supporting information online at https://www.pnas.org/lookup/suppl/doi:10.1073/pnas.2216887120/-/DCSupplemental.

Published March 15, 2023.

activates glial phagocytosis (27). Glia take up secreted APPL to maintain Drpr expression and up-regulate Rab GTPases, activating the glial endolysosomal network for the neuron clearance mechanism (27). Taken together, these studies suggest that neuronal FMRP interacts with neuronal InR, pMad, and pAkt signaling cascades to tightly regulate Prtp and APPL neuron-to-glia communication controlling the glial phagocytosis of target neurons during circuit remodeling in the juvenile brain.

Here, we use *Drosophila* brain PDF-Tri neuron removal via glial phagocytosis to study the neuron-to-glia communication remodeling mechanism, assaying both the early pruning steps at 1 day post-eclosion (dpe) and end-stage clearance (5 dpe) (18). We discover that neuronal FMRP binds *mad* mRNA to restrict pMad signaling in neurons. Surprisingly, however, we find that both neuronal *Drosophila fragile X mental retardation 1* (*dfmr1*) and *mad* RNAi similarly block PDF-Tri neuron removal, indicating a more complex regulatory mechanism. Consistently, we find pMad is a positive transcription factor for InRs driving downstream pAkt signaling but that pMad also indirectly inhibits pAkt, inducing the phenocopy between neuronal *dfmr1* and *mad* RNAi conditions. We find both neuronal *dfmr1* and *mad* RNAi similarly decrease Prtp neuron-to-glia signaling, resulting in reduced glial phagocytic activity and a block of PDF-Tri neuron clearance, whereas loss of neuronal InR and pAkt has that opposite phenotype of elevating Prtp to accelerate neuronal removal. We also discover that the FMRP-pMad-InR-pAkt pathway positively regulates neuronal APPL signaling to induce glial Rab7-driven endolysosomal activation for PDF-Tri neuron clearance. Taken together, we conclude that neuronal FMRP-pMad and InR-pAkt cascades coordinate an integrated regulatory decision network governing neuron-to-glia communication via neuronal Prtp and APPL signaling ligands that drive glial phagocytosis for targeted neuron pruning from brain circuits.

Results

Neuronal FMRP Regulates pMad Signaling to Mediate PDF-Tri Neuron Clearance. Previous genetic studies have shown that PDF-Tri neuron removal over the first 5 d in the early juvenile brain requires phagocytosis clearance by two cooperating glial subclasses (16, 19). To begin to dissect this mechanism further, we imaged interactions between glia and neurons early and late in this clearance process at 1 day posteclosion (dpe) and 5 dpe. To image neuron–glia interactions, we first used projected confocal microscopy to visualize glial localization relative to PDF-Tri neurons at 1 dpe during the early stages of the phagocytic removal (Fig. 1*A*). In 2D projections, the glia-specific reversed polarity (Repo) nuclear marker shows glial cells closely surrounding the PDF-Tri neurons, with multiple glia in direct contact along the entire length of the neuronal processes (Fig. 1 *B*, *Top*). In magnified three-dimensional (3D) reconstructed views, multiple glia (arrows) contact the PDF-Tri neuron, converging on the remodeling neurons from multiple directions (Fig. 1 *B*, *Bottom* and Movie S1). To label the glial membrane, we expressed UAS-mCD8::GFP with *repo*-Gal4 to show the PDF-Tri neuronal cell body covered by glial projections (Movie S2), further demonstrating close interaction between glia and PDF-Tri neurons. Previous studies have shown neuronal FMRP signals glial phagocytosis for PDF-Tri neuron removal (18). To test this mechanism over the time course of clearance, we assayed the PDF-Tri neuron area at 1 dpe (early in the removal process) and 5 dpe (at the end of the removal process) in neuronal driver controls (*elav*-Gal4/+) and with *dfmr1* RNAi (Fig. 1*C*). At 1 dpe, controls (*elav*/+) already show dramatically reduced PDF-Tri neuron area compared to *dfmr1* RNAi (*elav>dfmr1* RNAi) animals (Fig. 1*D*). Two-way ANOVA indicates that neuronal FMRP loss causes retention of significantly more PDF-Tri neuron area at 1 dpe. By the end of the removal process (5 dpe), controls show near-complete PDF-Tri neuron loss, whereas *dfmr1* RNAi results in neuron maintenance (Fig. 1*C*). The control PDF-Tri neuron area is enormously reduced compared to neuron retention with *dfmr1* RNAi, a highly significant difference by two-way ANOVA (Fig. 1*D*). To specifically test FMRP in PDF-Tri neurons, we assayed PDF driver controls (*PDF*-Gal4/+) alone and with targeted *dfmr1* RNAi (*SI Appendix*, Fig. S1*A*). FMRP loss in PDF neurons significantly lowers PDF-Tri neuron clearance at 1 dpe (*SI Appendix*, Fig. S1*B*). Taken together, these findings indicate that neuronal FMRP plays critical roles in driving normal PDF-Tri neuron clearance in the early juvenile brain.

We recently discovered that *dfmr1* null neurons accumulate high levels of phosphorylated mothers against decapentaplegic (pMad), indicating FMRP limits neuronal pMad signaling (24). To study this mechanism of FMRP-pMad regulation in the context of PDF-Tri neuron removal from the developing brain, we first tested pMad levels with neuronal *dfmr1* RNAi in staged brain western blot analyses (Fig. 1*E*). Comparisons with the neuronal driver controls (*elav*/+) show that *dfmr1* RNAi results in a consistently elevated pMad level. Quantified analyses indicate that neuronal *dfmr1* RNAi causes a significantly higher pMad signaling level, greater than twofold increase over the matched control (Fig. 1*F*). Since mouse RNA immunoprecipitation (RIP) sequencing has shown that FMRP binds *smad* mRNA (*Drosophila mad* homologue) (23), we next assayed for an RNA-binding interaction. To analyze FMRP-bound transcript levels, we used GFP-trap beads to pull down a FMRP::YFP fusion compared with a GFP-negative control from brain neurons (24). As FMRP has been shown to bind *staufen* (*stau*) mRNA (24), we use *stau* as the immunoprecipitation positive control (Fig. 1*G*). With quantitative real-time PCR (qPCR) measurements, we found a >1.5-fold immunoprecipitation enrichment for *mad* mRNA occurs with FMRP::YFP pull-down as normalized compared to the GFP-negative control (Fig. 1*G*). This is comparable to the approximately twofold immunoprecipitation for the *stau* positive control. These results show FMRP binds *mad* mRNA in brain neurons, so we next tested possible FMRP-dependent effects on *mad* transcription levels (Fig. 1*H*). Compared with the driver control (*elav*/+), reducing neuronal FMRP (*elav>dfmr1* RNAi) causes a significant increase in *mad* mRNA levels (Fig. 1*H*). This suggests that neuronal FMRP destabilizes bound *mad* transcripts to reduce the amount of protein produced. Taken together, these findings indicate that FMRP binds *mad* mRNA and reduces *mad* transcript levels, thereby presumably restricting pMad intracellular signaling.

During intracellular signaling, the phosphorylation of Mad (pMad) generates an active transcription factor that translocates into the nucleus to directly regulate gene expression (20). We therefore next wanted to determine whether knockdown of neuronal *mad* mRNA impairs pMad signaling and whether neuronal pMad signaling regulates targeted PDF-Tri neuron removal. To test the first question, we compared driver controls (*elav*/+) to neuronal *mad* RNAi (*elav>mad* RNAi) to find a significant reduction in pMad protein levels. To test whether neuronal pMad regulates PDF-Tri neuron clearance, we therefore reduced pMad in neurons by neuronal *mad* RNAi (Fig. 2*A*). Surprisingly, this knockdown results in impaired PDF-Tri neuron clearance similar to the *dfmr1* RNAi condition (compare to Fig. 1 *C* and *D*). Starting early in the glial clearance process (1 dpe), and particularly at the end of the removal mechanism when PDF-Tri neurons are normally absent (5 dpe), neuronal *mad* RNAi results

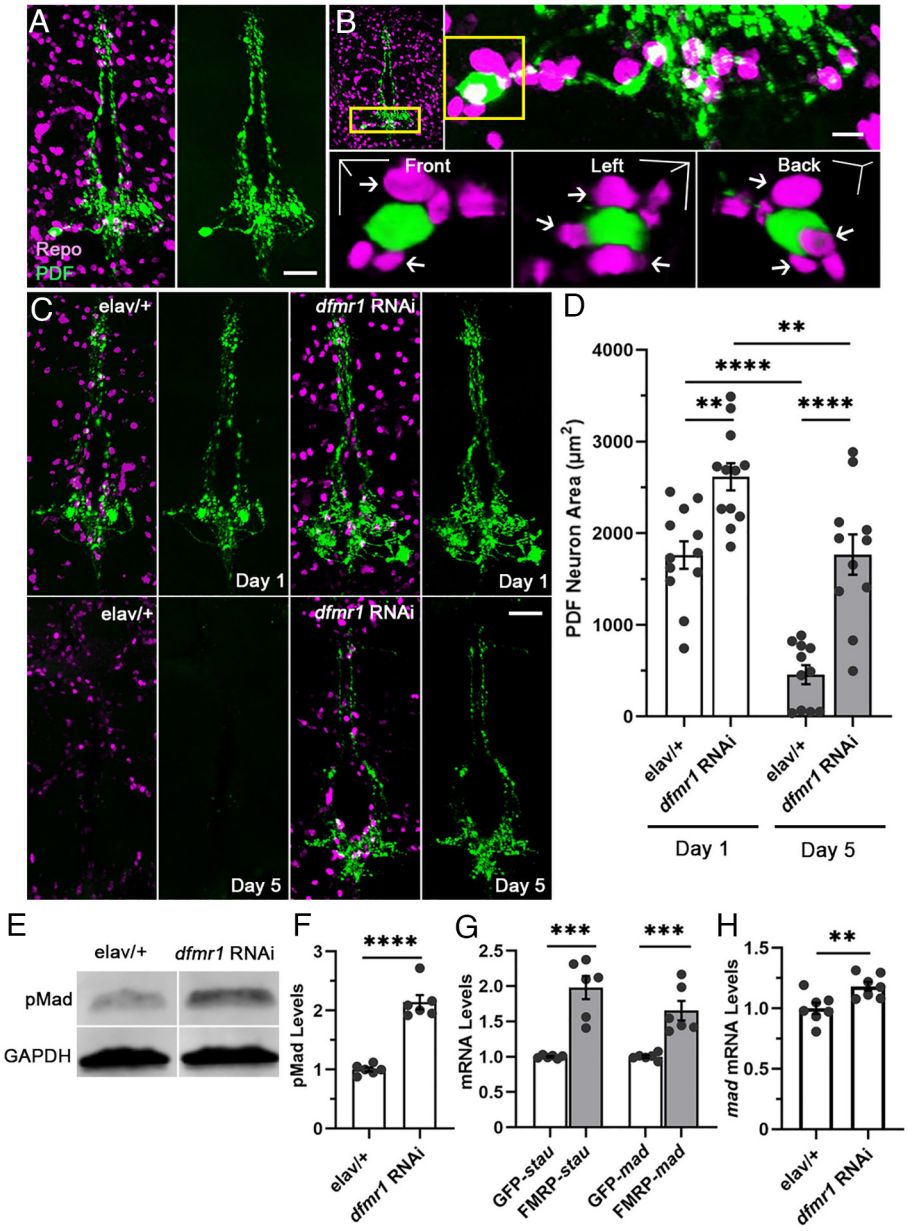

Fig. 1. Glial phagocytic removal of PDF-Tri neurons requires FMRP regulation of pMad. (*A*) PDF-Tri neuron (anti-PDF, green) and glial cells (anti-Repo, magenta) in the central brain at the early glial phagocytic removal (0-1 dpe). (Scale bar, 20 µm.) (*B*) Progressively higher magnified views of PDF-Tri neuron and glia interaction. [Scale bars, magnified 2D (*Right Top*), 5 µm; magnified 3D (*Right Bottom*), 5 µm on X, Y, and Z axes.] (*C*) Double labeling of the neuronal driver control (*elav/+*, *Left*) and with *dfmr1* RNAi (*Right*) at day 1 (*Top*) and day 5 (*Bottom*) after eclosion. (Scale bar, 20 µm.) (*D*) Two-way ANOVA of the PDF-Tri neuron area quantification at both time points (data shown as mean ± SEM; 1 dpe: control 1,761.0 ± 149.80 vs. *dfmr1* RNAi 2,615.0 ± 148.30, $P = 0.0047$; 5 dpe: control 455.9 ± 104.10 vs. *dfmr1* RNAi 1,767.0 ± 219.90, $P < 0.0001$). There is no significant difference in glia density between *elav/+* and *elav>dfmr1* RNAi ($P = 0.121$). (*E*) Representative anti-pMad western blot of neuronal *elav/+* control and with *dfmr1* RNAi. GAPDH is the loading control. (*F*) Normalized pMad levels from the western blots (control 1.00 ± 0.034 vs. *dfmr1* RNAi 2.14 ± 0.121; Student's *t* test, $P < 0.0001$). (*G*) RNA immunoprecipitation and normalized quantification of FMRP-bound transcripts. GFP-trap beads pull down neuronal YFP::FMRP together with negative control GFP (GFP-stau 1.00 ± 0.009 vs. FMRP-stau 1.979 ± 0.163, Student's *t* test, $P = 0.0001$; GFP-mad 1.00 ± 0.019 vs. FMRP-mad 1.653 ± 0.137, Student's *t* test, $P = 0.0008$). (*H*) Normalized *mad* mRNA levels in *elav/+* control and with *dfmr1* RNAi (control 1.00 ± 0.045 vs. *dfmr1* RNAi 1.182 ± 0.037, Student's *t* test, $P = 0.009$). Dot plots show all data points. Statistical significance indicated as $^{**}P < 0.01$, $^{***}P < 0.001$, and $^{****}P < 0.0001$.

in a striking retention of most of the neuronal architecture (Fig. 2*A*). Statistical analyses indicate that neuronal *mad* RNAi causes significantly reduced PDF-Tri neuron removal compared to driver controls (*elav/+*) at 1 dpe and an even stronger significant maintenance at 5 dpe (Fig. 2*B*). To specifically test FMRP in PDF-Tri neurons, we assayed PDF driver controls (*PDF-Gal4/+*) alone and with *mad* RNAi (PDF>*mad* RNAi; *SI Appendix*, Fig. S1*A*). Loss of pMad signaling in PDF neurons very significantly lowers PDF-Tri neuron clearance at 1 dpe (*SI Appendix*, Fig. S1*B*). Since this conclusion is opposite to expectations, a second FMRP-pMad interactive pathway was suspected to result in the *dfmr1* RNAi phenocopy. As both FMRP and pMad interact with insulin receptor (InR) signaling (19, 20, 29), we therefore next focused on testing InR dysregulation in neuronal *dfmr1* and *mad* RNAi conditions. With qPCR assays, InR expression is oppositely modulated by neuronal *dfmr1* and *mad* RNAi (Fig. 2 *C* and *D*), which fits the inhibitory regulation from FMRP to pMad. However, this fails to explain the phenocopy result. We therefore next explored interactions downstream of InR signaling.

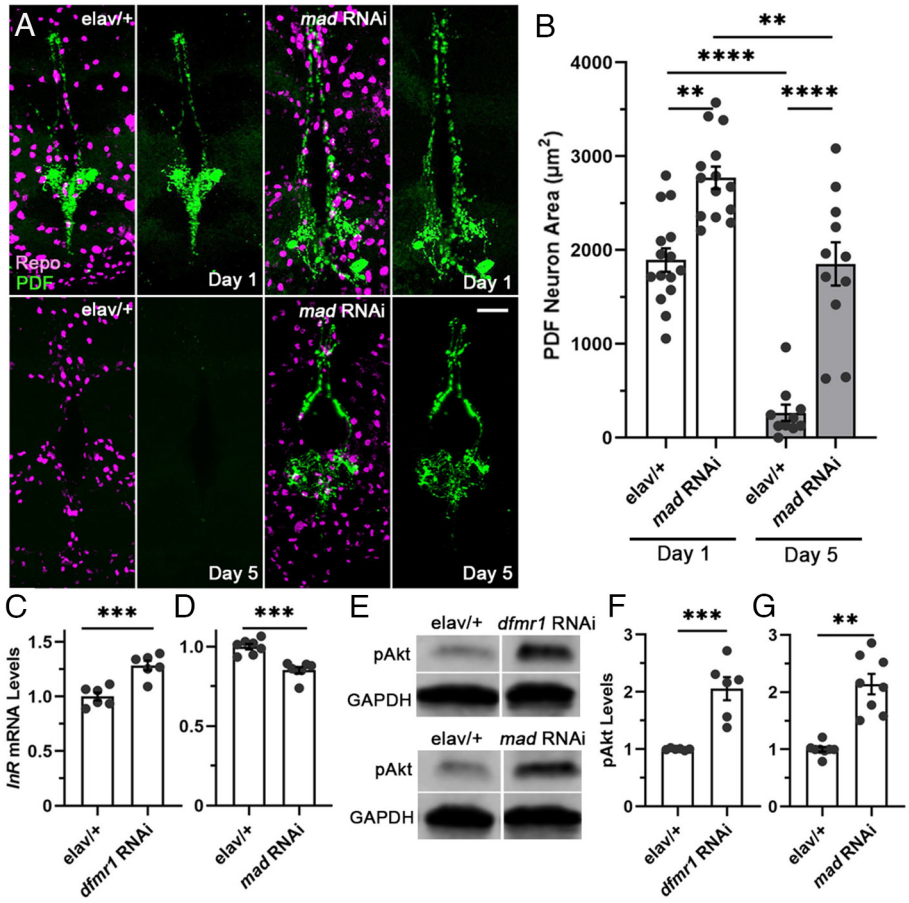

Fig. 2. PDF-Tri neuron clearance through FMRP-pMad signaling up-regulates pAkt level. (*A*) PDF-Tri neuron (green) and glia (magenta) labeling in the neuronal driver control only (*elav*/+, *Left*) and with neuronally driven *mad* RNAi (*Right*) at day 1 (*Top*) and day 5 (*Bottom*) after eclosion. PDF-Tri neuron alone is shown to the right for each image. (Scale bar, 20 μm.) (*B*) PDF-Tri neuron area quantification for both genotypes at both time points (1 dpe: control 1,894.0 ± 125.10 vs. *mad* RNAi 2,771.0 ± 118.60, two-way ANOVA, $P = 0.0020$; 5 dpe: control 265.20 ± 86.97 vs. *mad* RNAi 1,852.0 ± 230.80, two-way ANOVA, $P < 0.0001$). There is no significant difference in glia density (anti-Repo) between *elav*/+ and *elav*>*mad* RNAi ($P = 0.642$). (*C* and *D*) Normalized *InR* mRNA levels with the neuronal *elav*/+ driver control compared to *dfmr1* RNAi (*C*, *elav*/+ 1.00 ± 0.036 vs. *dfmr1* RNAi 1.283 ± 0.0441, Student's *t* test, $P = 0.0006$) and *mad* RNAi (*D*, *elav*/+ 1.00 ± 0.018 vs. *mad* RNAi 0.851 ± 0.020, Student's *t* test, $P = 0.0001$). (*E*) Representative anti-pAkt western blots with the neuronal *elav*/+ driver control compared to both neuronal *dfmr1* RNAi (*Top*) and neuronal *mad* RNAi (*Bottom*) conditions. GAPDH is the loading control. (*F* and *G*) Western blot quantification for both conditions compared to *elav*/+ driver control (*F*, *elav*/+ 1.00 ± 0.007 vs. *dfmr1* RNAi 2.06 ± 0.203, Student's *t* test, $P = 0.0004$; *G*, *elav*/+ 1.00 ± 0.041 vs. *mad* RNAi 2.14 ± 0.178, Student's *t* test, $P < 0.0001$). Dot plots show all data points. Statistical significance indicated as $^{**}P < 0.01$, $^{***}P < 0.001$, and $^{****}P < 0.0001$.

Activated InR phosphorylates protein kinase B (pAkt) (30, 31), and FMRP loss elevates pAkt in neurons (29). To test whether pAkt is the dysregulated player in the FMRP-pMad signaling, we first used western blots to measure pAkt levels in driver controls (*elav*/+) compared with *dfmr1* and *mad* RNAi (Fig. 2*E*). Quantification shows pAkt up-regulated by both neuronal *dfmr1* and *mad* RNAi, with a significantly approximately twofold enrichment in both cases (Fig. 2 *F* and *G*). To test pAkt in PDF-Tri neurons, we colabeled with anti-PDF and anti-pAkt. Both *dfmr1* and *mad* RNAi increase pAkt in PDF-Tri neurons at 1 dpe (*SI Appendix*, Fig. S1 *C–E*). These findings suggest pAkt upregulation generates the neuronal *dfmr1* and *mad* RNAi phenocopy blocking PDF-Tri neuron removal. Consistently, neuronal pAkt RNAi dramatically increases the rate of PDF-Tri neuron clearance (Fig. 3*A*). Due to the complete neuron loss at 5 dpe in controls, we only measured the PDF-Tri neuron area at 1 dpe to show significantly accelerated neuronal removal early in the process (Fig. 3*B*). As decreasing neuronal pMad results in aberrant pAkt elevation, we hypothesized that correcting neuronal pAkt levels in the reduced pMad background should restore normal clearance. With *mad* and *akt* double RNAi, PDF-Tri neuron clearance is restored to control levels (Fig. 3 *C* and *D*), supporting this hypothesis. To test possible Gal4 dilution with double UAS constructs, we also expressed *akt* RNAi with control *gfp* RNAi. This double RNAi still significantly promotes neuron loss (*SI Appendix*, Fig. S2 *A* and *B*). We also overexpressed *akt* (*elav*>*akt* OE) to find slower PDF-Tri neuron loss at 1 dpe (*SI Appendix*, Fig. S2 *C* and *D*). PDF-Tri neuron clearance defects from *InR* knockdown (Fig. 3 *E* and *F*) and constitutive activation (InR CA; *SI Appendix*, Fig. S2 *C* and *D*) are also consistent with InR acting as a positive regulator to pAkt (31). Importantly, *InR* and *akt* RNAi cause no significant effect on PDF-Tri neurons in pre-eclosion pharate adults (*SI Appendix*, Fig. S3 *A–D*), supporting a specific role for InR-pAkt signaling in PDF-Tri neuron clearance. We finally tested InR-pAkt signaling within PDF-Tri neurons. Consistent with pan-neuronal RNAi, both PDF-Gal4-driven *InR* and *akt* RNAi promote PDF-Tri neuron clearance, while targeted *akt* and *mad* double RNAi correct the *akt* phenotype (*SI Appendix*, Fig. S4 *A* and *B*). These results show FMRP-pMad cross talk to InR-pAkt signaling regulates PDF-Tri neuron removal. However, this intracellular neuronal network must act to control intercellular signaling to drive glial phagocytosis, so we next turned to testing the neuron-to-glia communication mechanism.

Neuronal FMRP-pMad-InR Network Regulates Pretaporter Signaling for Glial Phagocytosis. Neuronal pretaporter (Prtp) binds the glial draper engulfment receptor to drive the glial phagocytosis of neurons (26). Neurons traffic Prtp from the endoplasmic reticulum (ER) to the plasma membrane cell surface to activate targeted glial phagocytosis (26). We therefore next tested neuronal

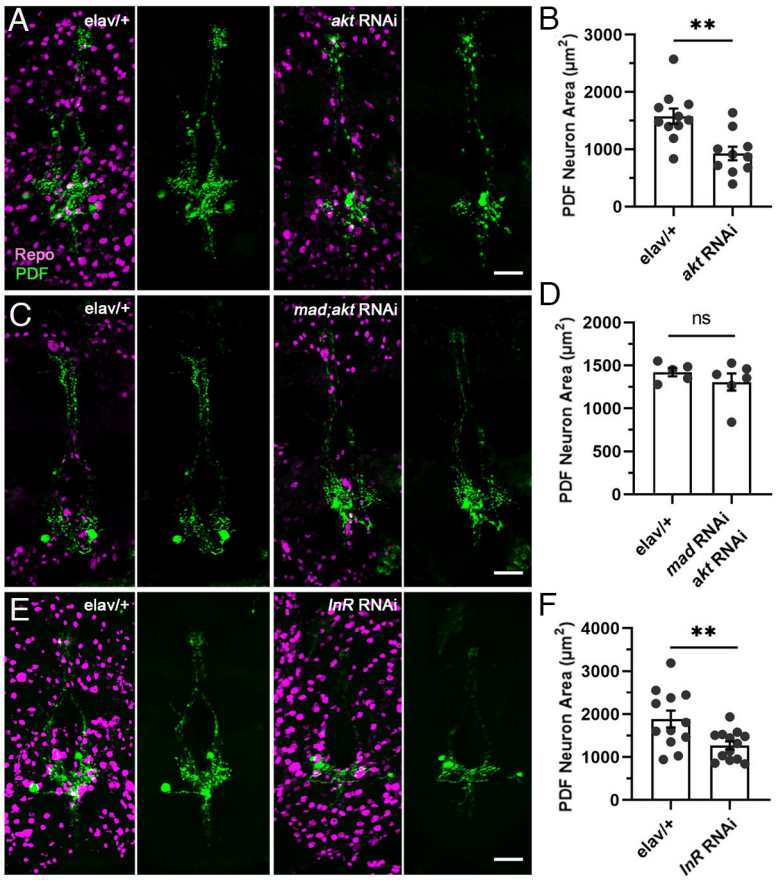

Fig. 3. Neuronal knockdown of both InR and Akt accelerates PDF-Tri neuron clearance. (*A*) PDF-Tri neuron (anti-PDF, green) and glia (anti-Repo, magenta) double labeling in the neuronal driver control (*elav*/+, *Left*) and *akt* RNAi (*Right*) at day 1 posteclosion during the early stages of the glial phagocytic removal process. (Scale bar, 20 µm.) (*B*) Quantification of the PDF-Tri neuron area in the two conditions (*elav*/+ 1,578.0 ± 132.0 vs. *akt* RNAi 927.10 ± 117.70, Students' *t* test, $P = 0.0017$). There is no significant difference in glia density between *elav*/+ and *elav>akt* RNAi at 1 dpe ($P = 0.778$). (*C*) The same colabeling with neuronal *mad* and *akt* RNAi driven in double knockdown combination at day 1. (Scale bar, 20 µm.) (*D*) Quantification of the PDF-Tri neuron area in the two conditions (*elav*/+ 1424.0 ± 48.69 vs. *mad*; *akt* double RNAi 1,308.0 ± 100.10, Students' *t* test, $P = 0.357$). (*E*) PDF-Tri neuron and glia double labeling in the neuronal driver control (*elav*/+, *Left*) and with *InR* RNAi (*Right*) at day 1. (*F*) Quantification of the PDF-Tri neuron area in the two conditions (*elav*/+ 1,886.0 ± 196.10 vs. *InR* RNAi 1,273.0 ± 94.27, Students' *t* test, $P = 0.008$). There is no significant difference in glia density between *elav*/+ and *elav>InR* RNAi at 1 dpe ($P = 0.464$). Dot plots show all data points. Statistical significance indicated as $^{**}P < 0.01$ and not significant (ns; $P > 0.05$). (Scale bar in all images, 20 µm.)

Prtp knockdown (*elav>prtp* RNAi) compared to the driver control (*elav*/+) to test whether PDF-Tri neuron removal involves Prtp signaling (Fig. 4*A*). In assaying the full time course of the glial phagocytosis mechanism, we find strongly reduced PDF-Tri neuron clearance at both 1 dpe (early) and 5 dpe (late) with neuronal Prtp knockdown (Fig. 4*A*). As usual, the aberrant retention is more obvious at 5 dpe, although the PDF-Tri neuron maintenance here is reduced relative to both the *dfmr1* and *mad* RNAi conditions (compare to Figs. 1 and 2), suggesting the combinatorial action of parallel neuron-to-glia signals (see below). Two-way ANOVAs show the PDF-Tri neuron area with neuronal *prtp* RNAi is significantly greater early in the glial removal process (1 dpe) and also at the end of clearance (5 dpe) when neurons are normally eliminated in the *elav*/+ driver controls (Fig. 4*B*). These results suggest neuronal Prtp is involved in PDF-Tri neuron clearance by inducing glial phagocytosis. We therefore next tested whether the above neuronal FMRP-pMad and InR-pAkt network modulates Prtp signaling. With qPCR assays, both neuronal *dfmr1* and *mad* RNAi reduce *prtp* levels (Fig. 4 *C* and *D*), consistent with the inhibition of PDF-Tri neuron clearance. Moreover, both neuronal *InR* and *akt* RNAi elevate *prtp* levels (Fig. 4 *E* and *F*), consistent with accelerated PDF-Tri neuron clearance. These combined interactions provide a mechanism to explain the bidirectional change in PDF-Tri neuron removal in these two pathway conditions downstream of the linked neuronal regulation. Taken together, these findings show the neuronal FMRP-pMad and InR-pAkt network controls Prtp signaling to regulate the glial phagocytic clearance of PDF-Tri neurons. However, another neuron-to-glia intercellular signaling mechanism seemed to be acting in parallel.

Neuronal FMRP-pMad and InR-pAkt Network Regulates Amyloid Precursor Protein Signaling. In the mouse FXS model, FMRP restricts neuronal amyloid precursor protein (APP) levels (32, 33). In *Drosophila*, the amyloid precursor protein-like (APPL) homologue cleaved N terminus released from brain neurons is engulfed by glia to activate their phagocytic function during brain neuron removal (27). To test whether neuronal APPL is required for PDF-Tri neuron clearance, we next compared driver controls (*elav*/+) with neuronal APPL knockdown (*elav>appl* RNAi) at 1 dpe (early) and 5 dpe (late) in the glial phagocytosis clearance process (Fig. 5*A*). Brain imaging shows more PDF-Tri neuron retention with neuronal *appl* RNAi compared to driver controls at 1 dpe and 5 dpe, with the difference more obvious late in glial removal (Fig. 5*A*). Quantification shows the removal of PDF-Tri neurons is significantly reduced with neuronal *appl* RNAi at both the 1 dpe and 5 dpe time points (Fig. 5*B*). These results are consistent with recently reported APPL requirements in glia-mediated neuronal removal (27). We next tested if FMRP and APPL interact to regulate PDF-Tri neuron removal. Single *dfmr1*/+ and $appl^{d}$/+ heterozygotes have no significant impact on PDF-Tri neuron clearance compared to

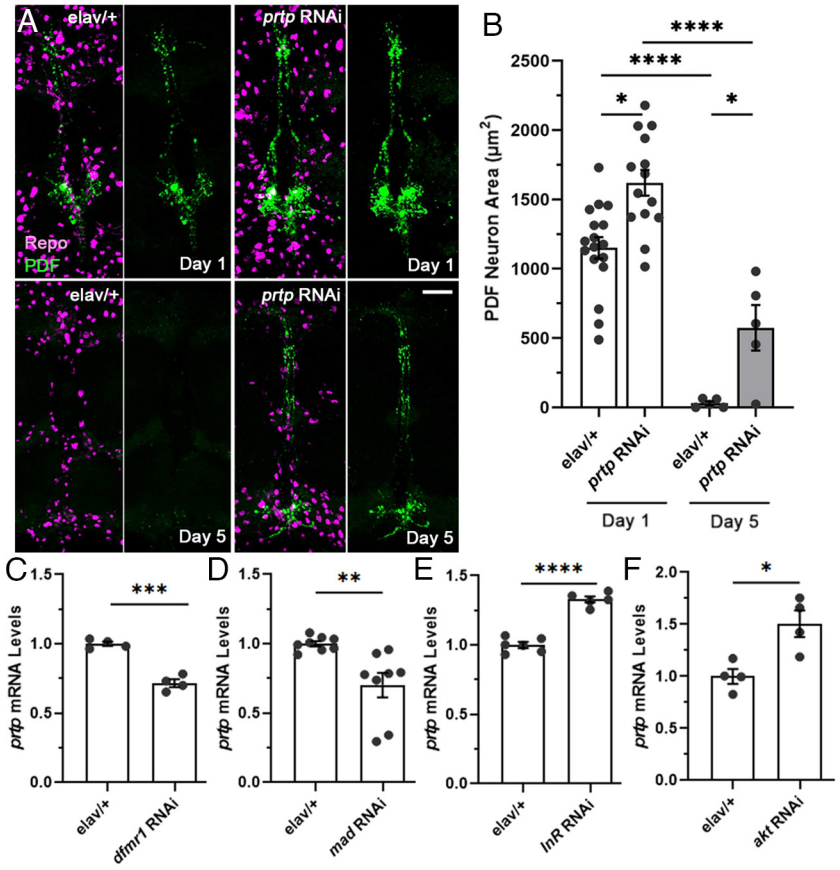

Fig. 4. Neuron-to-glia pretaporter signaling acts downstream of FMRP, pMad, and InR. (*A*) PDF-Tri neuron (green) and glia (magenta) colabeling with the neuronal driver control (*elav*/+, *Left*) and neuronal *pretaporter* RNAi (*prtp*, *Right*) at both day 1 (*Top*) and day 5 (*Bottom*). (Scale bar, 20 µm.) (*B*) Quantification of the PDF-Tri neuron area for both the genotypes at both early and late time points (1 dpe: *elav*/+ 1,151.0 ± 77.48 vs. *prtp* RNAi 1,620.0 ± 93.28, two-way ANOVA, $P = 0.0148$; 5 dpe: *elav*/+ 29.51 ± 14.21 vs. *prpt* RNAi 574.0 ± 164.10, two-way ANOVA, $P = 0.0432$). There is no significant difference in glia density between *elav*/+ and *elav*>*prtp* RNAi ($P = 0.571$). (*C*) Normalized quantification of *prtp* mRNA levels in the neuronal driver control (*elav*/+, *Left*) and with neuronal *dfmr1* RNAi (*Right*) (*elav*/+ 1.00 ± 0.016 vs. *dfmr1* RNAi 0.717 ± 0.027, Students' *t* test, $P = 0.0001$). (*D*) Normalized quantification of *prtp* mRNA levels in the neuronal driver control (*elav*/+, *Left*) and with neuronally targeted *mad* RNAi (*Right*) (*elav*/+ 1.00 ± 0.018 vs. *mad* RNAi 0.702 ± 0.089, Students' *t* test, $P = 0.0051$). (*E*) Normalized quantification of *prtp* mRNA levels in the neuronal driver control (*elav*/+, *Left*) and with neuronal *InR* RNAi (*Right*) (*elav*/+ 1.00 ± 0.021 vs. *InR* RNAi 1.329 ± 0.022, Students' *t* test, $P < 0.0001$). (*F*) Normalized quantification of *prtp* mRNA levels in the neuronal driver control (*elav*/+, *Left*) and with neuronal *akt* RNAi (*Right*) (*elav*/+ 1.00 ± 0.07045 vs. *InR* RNAi 1.507 ± 0.127, Students' *t* test, $P = 0.0130$). Dot plots show all data points. Statistical significance indicated as $*P < 0.05$, $**P < 0.01$, $***P < 0.001$, and $****P < 0.0001$.

the genetic background control w^{1118}, whereas the *dfmr1*/+; $appl^{d}$/+ *trans*-heterozygote significantly increases PDF-Tri neuron retention (*SI Appendix*, Fig. S5 *A* and *B*). To investigate how neuronal FMRP-pMad and InR-pAkt signaling might regulate this APPL function, we next combined qPCR and western blots to measure APPL expression in targeted RNAi studies for neuronal *dfmr1*, *mad,* and *InR* RNAi (Fig. 5 *C–E*). Quantified analyses show a similar significant reduction in *appl* transcript levels with both *dfmr1* and *mad* RNAi compared to the *elav*/+ driver controls (Fig. 5 *C* and *D*), consistent with the PDF-Tri neuron persistence in both these conditions. Likewise, neuronal *InR* knockdown results in an even more significant ~50% reduction in *appl* mRNA levels (Fig. 5*E*). Moreover, neuronal *dfmr1*, *mad*, *InR,* and *akt* RNAi also decrease APPL protein levels (Fig. 5*F*). The *dfmr1* and *mad* results are again consistent with the delayed neuronal removal, but the decreased APPL with *InR* and *akt* RNAi opposes the phenotype of accelerated PDF-Tri neuron removal. Taken together, neuronal FMRP-pMad and InR-pAkt cascades similarly regulate neuronal APPL levels. However, we still wished to test the role of neuronal signaling in glial activation for PDF-Tri neuron removal.

Neuronal FMRP-pMad and InR-pAkt Network Up-Regulates Glial Endolysosomal Activity. Neuronal InR signaling inhibits glial engulfment (34, 35), with reduced endolysosomal activation in glia (36). The APPL N terminus released from brain neurons up-regulates the glial Rab GTPases endolysosomal network for glial phagocytosis (27). Thus, the InR-pAkt-APPL regulation of glial activation has been established. To test whether neuronal FMRP-dependent pMad and Prtp signaling plays roles in transcellularly regulating glial endolysosomal activation, two binary transgenic systems were used in parallel: 1) neuron-targeted RNAi lines driven with Gal4/UAS, and 2) glia-targeted mCD8::GFP plasma membrane labeling with LexA/LexAOP (Fig. 6*A*). All assays were done on glia immediately adjacent to the PDF-Tri neuron cell bodies at 1 dpe to investigate early-stage activation in the pruning glial population. As endolysosomal sorting starts with the Rab5 GTPase in early endosomes (27, 37), we first tested anti-Rab5 labeling in glia. None of the neuronal RNAi manipulations cause any change in the glial Rab5 signal, indicating early endosomal activity is not affected. Late endolysosomal sorting employs the Rab7 GTPase on late endosomes and lysosomes (27), so we next tested anti-Rab7 labeling in glia. Neuronal *dfmr1*, *mad,* and *prtp* RNAi all dramatically depress glial Rab7 (Fig. 6*A*). The driver controls (*elav*/+) consistently have larger, more numerous Rab7 puncta in glia adjacent to the PDF-Tri neurons, whereas all three neuronal knockdowns (*dfmr1*, *mad,* and *prtp* RNAi) have obviously smaller Rab7 puncta that are relatively difficult

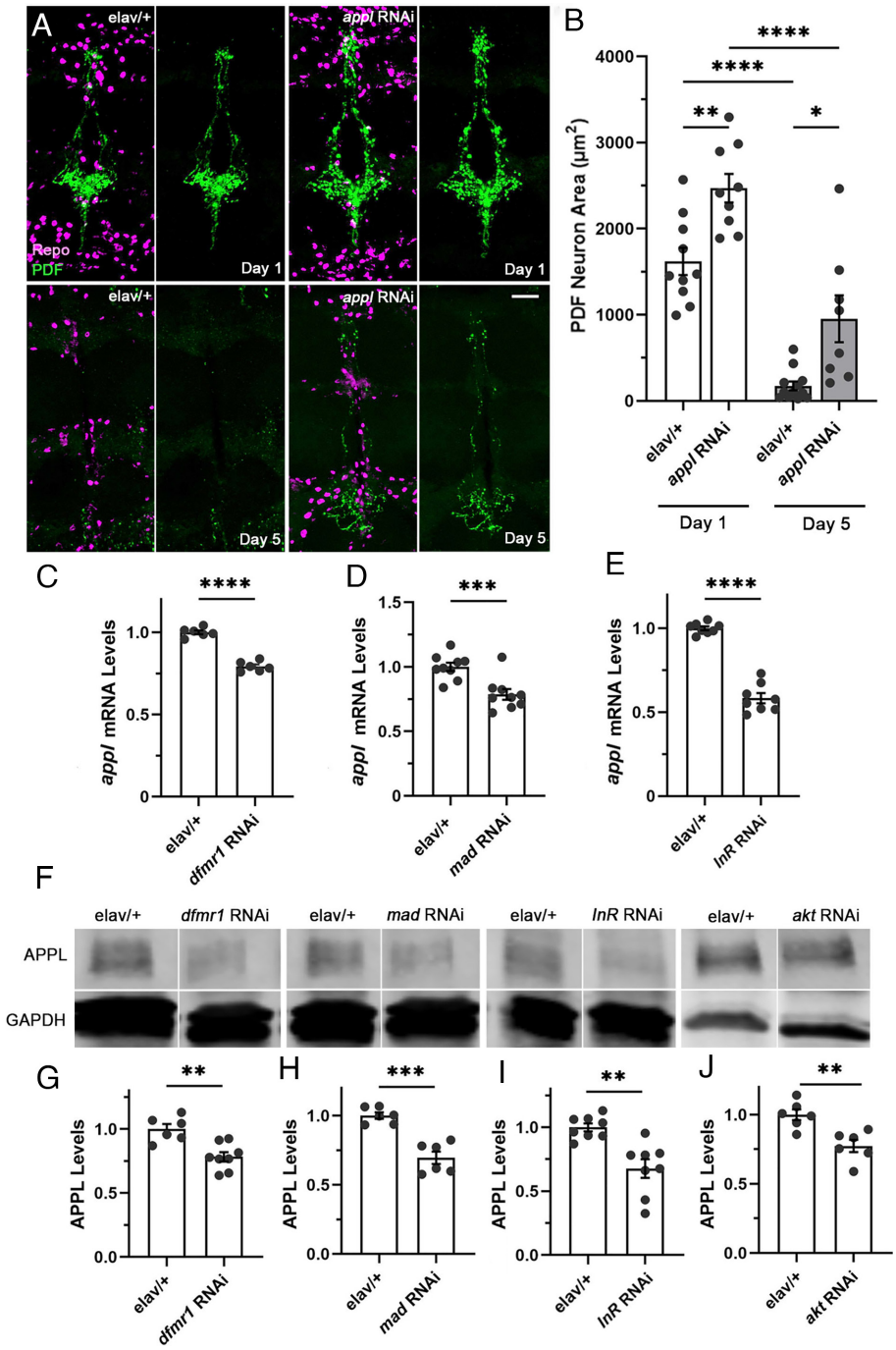

Fig. 5. Neuronal APPL acts in the same pathway to facilitate PDF-Tri neuron clearance (*A*) PDF-Tri neuron (anti-PDF, green) and glial cell (anti-Repo, magenta) double labeling in the neuronal driver control (*elav/+*, *Left*) and *appl* RNAi (*Right*) at both day 1 (*Top*) and day 5 (*Bottom*). The PDF-Tri neuron alone (green) is shown to the *Right*. (Scale bar, 20 μm.) (*B*) Quantification of the PDF-Tri neuron area for both genotypes at both early and late time points (1 dpe: *elav/+* 1,620.0 ± 158.70 vs. *appl* RNAi 2,469.0 ± 165.40, two-way ANOVA, $P = 0.0072$; 5 dpe: *elav/+* 175.0 ± 51.34 vs. *appl* RNAi 954.0 ± 272.50, two-way ANOVA, $P = 0.0195$). There is no significant difference in glia density between *elav/+* and *elav>appl* RNAi ($P = 0.746$). (*C–E*) Normalized quantification of *appl* mRNA levels in neuronal driver controls (*elav/+*, *Left*) compared with neuronal *dfmr1* RNAi (*C*, *elav/+* 1.00 ± 0.012 vs. *dfmr1* RNAi 0.79 ± 0.013, Students' *t* test, $P < 0.0001$), *mad* RNAi (*D*, *elav/+* 1.00 ± 0.032 vs. *mad* RNAi 0.70 ± 0.042, Students' *t* test, $P = 0.0009$), and *lnR* RNAi (*E*, *elav/+* 1.00 ± 0.011 vs. *lnR* RNAi 0.58 ± 0.030, Students' *t* test, $P < 0.0001$). (*F*) Representative anti-APPL western blots with the neuronal *elav/+* controls (*Left* in each pairing) and neuronal *dfmr1* RNAi (*Left*), *mad* RNAi (second from *Left*), *lnR* RNAi (second from *Right*), and *akt* RNAi (*Right*). (*G–J*) Western blot quantification normalized to neuronal *elav/+* controls (*Left* in each pairing) for *dfmr1* RNAi (*G*, *elav/+* 1.00 ± 0.039 vs. *dfmr1* RNAi 0.78 ± 0.037, Students' *t* test, $P = 0.0018$), *mad* RNAi (*H*, *elav/+* 1.00 ± 0.024 vs. *mad* RNAi 0.69 ± 0.045, Students' *t* test, $P = 0.0001$), *lnR* RNAi (*I*, *elav/+* 1.00 ± 0.031 vs. *lnR* RNAi 0.68 ± 0.073, Students' *t* test, $P = 0.0011$), and *akt* RNAi (*J*, *elav/+* 1.00 ± 0.040 vs. *akt* RNAi 0.77 ± 0.045, Students' *t* test, $P = 0.0037$). Dot plots show all data points. Statistical significance indicated as $*P < 0.05$, $**P < 0.01$, $***P < 0.001$, and $****P < 0.0001$.

to detect (Fig. 6*A*). Quantification of glial Rab7 volume shows the most significant reduction with neuronal *dfmr1* RNAi normalized to the *elav/+* control (Fig. 6*B*). Consistent with the above regulatory pathway, both neuronal *mad* and *prtp* RNAi also exhibit significantly reduced glial Rab7 volume during PDF-Tri neuron removal (Fig. 6 *C* and *D*). Together with established neuronal InR and APPL signaling of glial activation (29, 34–36), these findings show neuronal FMRP-pMad-Prtp signaling triggers glial endolysosomal phagocytosis activation for neuron clearance in the juvenile brain.

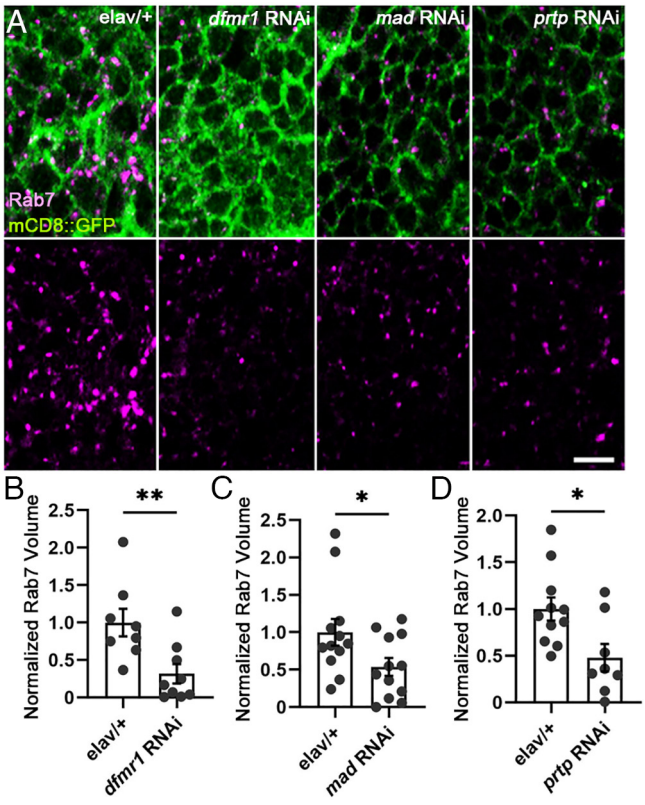

Fig. 6. Neuronal FMRP-pMad-Prtp signaling activates the glial endolysosomal pathway. (*A*) Glial cells immediately adjacent to the PDF-Tri neurons in the central brain marked with membrane mCD8::GFP (green) and colabeled with endolysosomal anti-Rab7 (magenta) at day 1 during the glial phagocytic removal process. The neuronal driver control alone (*elav/+*, *Left*) is compared to driven *dfmr1* RNAi (second from *Left*), *mad* RNAi (second from *Right*), and *prtp* RNAi (*Right*). The endolysosomal Rab7 is shown alone in the bottom row for all four genotypes. (Scale bar, 20 μm.) (*B–D*) Glial Rab7 volume normalized to the neuronal driver control (*elav/+*, *Left* in each pairing) compared to neuronal *dfmr1* RNAi (*B*, *elav/+* 1.00 ± 0.186 vs. *dfmr1* RNAi 0.318 ± 0.129, Students' *t* test, $P = 0.0078$), neuronal *mad* RNAi (*C*, *elav/+* 1.00 ± 0.178 vs. *mad* RNAi 0.537 ± 0.119, Students' *t* test, $P = 0.041$), and neuronal *prtp* RNAi (*D*, *elav/+* 1.00 ± 0.123 vs. *prtp* RNAi 0.479 ± 0.147, Students' *t* test, $P = 0.014$). Dot plots show all data points. Statistical significance indicated as $*P < 0.05$ and $**P < 0.01$.

Discussion

We have discovered an integrated mechanism of neuronal FMRP-dependent network signaling that regulates neuron-to-glia communication to drive the glial phagocytic removal of targeted neurons from an otherwise maintained brain circuit. Specifically, within the neurons, RNA-binding FMRP restricts the translation of bound *mad* transcripts to limit phosphorylated Mad (pMad) signaling, which, in turn, inhibits phosphorylated Akt (pAkt) to promote glial phagocytosis for neuron removal. In parallel, the neuronal insulin receptor (InR) regulates pAkt signaling in a second intersecting cascade controlling the neuronal clearance mechanism. This bone morphogenic protein (BMP) and insulin-like peptide (ILP) neural decision-making network (19) controls neuron-to-glia communication regulating glial phagocytosis function for targeted neuron removal. Neuronal pretaporter (Prtp) is a ligand for the draper (Drpr) engulfment receptor on glia (26). The FMRP-pMad pathway promotes neuron-to-glia Prtp signaling to induce glial phagocytosis for neuron clearance, whereas the InR-pAkt pathway suppresses Prtp signaling to repress glia-mediated neuron removal. Neuronal amyloid precursor protein like (APPL) is released via a cleavable N terminus to activate Rab7 GTPase endolysomes in glia (27). The FMRP-pMad regulatory pathway promotes this neuron-to-glia APPL signaling, consistent with inducing glial phagocytosis for neuron clearance, and the intersecting InR-pAkt pathway also up-regulates this signaling, suggesting additional roles in neuron removal. Overall, these findings indicate neuronal FMRP coordinates signal transduction cascades to provide cross talk downstream of two signaling inputs (BMP and ILP), which provides output in the form of two neuron-to-glia signaling ligands (Prtp and APPL) that regulate glial phagocytosis for the clearance of targeted neurons from the juvenile brain.

From mRNA Transcription to Phosphorylated Protein Signaling. We suggest RNA-binding FMRP limits pMad signaling levels by reducing the number of *mad* transcripts available for translation. FMRP is established to maintain protein translational homeostasis by modulating RNA target stability (38, 39). Ribosome profiling and transcriptome sequencing demonstrate imbalanced FMRP-targeted mRNA levels are common in the mouse FXS model brain due to reduced stabilization (38). In mouse RNA immunoprecipitation (RIP) sequencing, FMRP binds *smad* (*Drosophila mad* homologue) transcripts widely in the 5′-UTR, within the coding region, and in the 3′-UTR (23). With both RIP and qPCR measurements, we find *Drosophila* FMRP likewise binds *mad* mRNA and that FMRP loss increases both *mad* transcripts and pMad protein levels within brain neurons. We therefore suggest a causal effect correlation, although other indirect regulatory mechanisms are also possible (40, 41). We find loss of neuronal pMad decreases InR levels but elevates InR-dependent pAkt signaling, suggesting cross talk inhibition from pMad to pAkt. The pMad transcription factor (20) positively regulates InR expression. Downstream of the InR, pAkt regulates numerous targets, including target of rapamycin complexes (42) and the transcription factor forkhead box O (43), to regulate cell fate decisions (44, 45). In the brain neuronal fate decision, we suggest pMad inhibits pAkt signaling as a major cross talk regulation within the neuron-to-glia signaling network. With western blot assays, we find reducing neuronal pMad levels causes no changes in Akt protein levels but a approximately twofold increase in pAkt signaling. Thus, FMRP-dependent pMad signaling modulates InR-pAkt signaling at two levels: as a positive transcription factor regulating InR expression and as an inhibitor of downstream pAkt signaling. We conclude this cross talk provides critical regulation for targeted neuron pruning from the juvenile brain.

Brain Circuit Pruning in Fragile X Syndrome (FXS). Neuron removal from brain circuits is a normal mechanism in neurodevelopment, often mediated by glial phagocytosis (46–48). During the clearance process, glia engulf neurons and degrade internalized debris in endolysosomes (49, 50). In glia, the engulfed neuronal debris is first sorted in Rab5 GTPase early endosomes (27), then trafficked from early-to-late endosomes with accompanying increased intravacuolar acidification, and finally delivered to Rab7 GTPase lysosomes where acid hydrolases complete the degradation process (51). In both rodent and *Drosophila* FXS disease models, this glial phagocytosis mechanism is severely impaired, resulting in a failure to prune neurons in brain circuits (18, 52). In the *Drosophila* FXS model, loss of neuronal FMRP decreases the glial Drpr engulfment receptor, and loss of glial Drpr blocks glial phagocytosis to prevent neuron removal (18). This previous study generated the hypothesis that the impaired brain circuit neuron removal in the FXS disease model is caused by the loss of neuron-to-glia communication driving glial phagocytosis (15). With neuron-specific RNAi trials, we find the neuronal FMRP-pMad pathway triggers Drpr ligand Prtp signaling from neurons to mediate glial engulfment and phagocytosis, whereas the neuronal InR-pAkt pathway represses Prtp to oppose the glial removal mechanism. Furthermore, we find

targeted knockdown of neuronal FMRP, pMad, and Prtp impedes glial endolysosomal activation with reduced Rab7 expression, showing the neuronal FMRP-dependent network is required for glial phagocytosis function. These findings are consistent with the impaired glia-mediated neuron pruning in FXS disease models (18, 52) and provide insight into the molecular mechanisms of this defect. Clearly, the decision to eliminate neurons by glial phagocytosis rests on multiple, distinct signaling inputs and is executed via parallel avenues of neuron-to-glia communication.

Neuronal Prtp vs. APPL Regulation of Glial Phagocytosis. We find that loss of either neuronal Prtp or APPL hampers glial phagocytosis neuron removal from the juvenile brain circuit but that loss of either signal alone causes a less severe impairment than blocking the neuronal FMRP-pMad pathway. These results suggest that Prtp and APPL act combinatorially downstream of FMRP-pMad, consistent with both neuronal Prtp and APPL driving the glial phagocytic clearance of targeted neurons (26, 27). Prtp is a transmembrane protein trafficked from the endoplasmic reticulum (ER) to the cell surface of a neuron thus marked for removal, where it binds the Drpr engulfment receptor on glia (26). Through this mechanism, Prtp surface presentation downstream of the neuronal FMRP-pMad pathway is proposed to directly signal glial engulfment. In contrast, the cleaved extracellular domain of transmembrane APPL from neurons activates the glial endolysosomal network (27). This provides a separable function for APPL, suggesting why two signaling ligands mediate neuron removal by the glial phagocytosis mechanism. The Prtp signaling changes closely match the neuron clearance phenotypes of all neuronal *dfmr1*, *mad*, *InR,* and *akt* RNAi experiments. Likewise, the APPL signaling changes are consistent with FMRP-pMad regulation but not the InR-pAkt pathway. We therefore propose Prtp and APPL coregulate glial phagocytic activity with different strengths or independently participate in glial phagocytosis via other regulatory mechanisms. To test the possibility that Prtp interacts with APPL in this clearance mechanism, we could test the putative cross talk interaction at molecular and/or genetic levels. Conversely, neuronal Prtp and APPL may be independent signals in neuron-to-glial communication linked predominantly or solely through upstream FMRP regulation. Future studies will dissect these combinatorial signals downstream of inputs targeting the clearance of neurons from the juvenile brain.

Neuronal InR vs. Glial InR Roles in Glial Phagocytosis. The pigment-dispersing factor (PDF) brain circuit mediates circadian clock functions, with the developmentally transient central PDF-Tri neurons presumably driving eclosion timing (15). Multiple signals appear to coordinate the targeted clearance of PDF-Tri neurons from the juvenile brain, including insulin-like peptide (ILP) signaling (18). The insulin receptor (InR) is present in both neurons and glia, acting to coordinate intercellular communication and neuronal remodeling (1, 22, 53–55). For glial signaling, InRs are proposed to be activated by secreted ILPs from the remodeling neurons to stimulate transduction cascades promoting glial phagocytosis (18, 54). Glial InR phosphorylation triggers pAkt production, which, in turn, elevates Drpr engulfment receptor levels to drive glial phagocytosis (54). Consistently, genetically increasing glial InR levels elevates glia-dependent neuron removal of the PDF-Tri neurons (18). In the *Drosophila* FXS disease model, loss of FMRP represses InR phosphorylation in glia, whereas glial InR activation restores PDF-Tri neuron pruning (18). For neuron signaling, we propose that InR-mediated pAkt signal transduction regulates neuron-to-glia communication in this same remodeling process. Similarly, InR signaling in *Drosophila* dendrite arborization neurons inhibits their developmental pruning (22). Our work shows neuronal InR loss elevates Prtp signaling to drive glial phagocytosis, thus accelerating PDF-Tri neuron clearance from the juvenile brain. Neuronal InRs may be responding to autocrine ILP signaling from the remodeling neurons (18, 54) or ILPs from another source which is coordinating neuron and glia functions to properly regulate the glial phagocytosis neuron removal process. Future work will investigate how the different intercellular signals act on both neurons and glia to ensure the exact targeting and timing of the coordinated PDF-Tri neuron clearance from the juvenile brain.

Materials and Methods

***Drosophila* Genetics.** All *Drosophila* stocks were reared on cornmeal/agar/molasses food at 25 °C. Loss-of-function mutants used include $dfmr1^{50M}$ (24) and $appl^{d}$ Bloomington *Drosophila* Stock Center (BDSC# 43632) alleles (27). Transgenic drivers used include pan-neuronal *elav*-Gal4 (24), PDF-Gal4 (BDSC# 6899) (18), and glial *repo*-LexA (BDSC# 67096) (56). The controls include the w^{1118} genetic background (24) and the transgenic drivers alone. All genetic crosses and recombinations to make double transgenic insertions were performed with standard methods. Transgenic stocks were obtained from the Bloomington *Drosophila* Stock Center (BDSC) and are listed in *SI Appendix*, Table S1. UAS lines alone have been tested to show no significant effect on the PDF-Tri neuron phenotype (*SI Appendix*, Fig. S6 *A–C*).

Immunocytochemistry. Brains from synchronized, staged animals were dissected in phosphate-buffered saline (PBS), fixed in 4% paraformaldehyde in PBS for 30 min at room temperature (RT), and then blocked for 1 h at RT in PBS with 0.2% Triton X-100 (PBST) + 1% bovine serum albumin. Primary antibodies were diluted in the blocking buffer for incubation overnight at 4 °C, followed by washing 3X with PBST. Secondary antibodies were incubated for 3 h at RT and then washed 3X with PBST. Primary antibodies used were mouse anti-PDF [Developmental Studies Hybridoma Bank (DSHB), PDF C7,1:50], rabbit anti-Repo (gift from Dr. Benjamin Altenhein, University of Cologne, Germany, 1:1,000), chicken anti-GFP (Abcam, ab13970, 1:1,000), rabbit anti-Rab5 (Abcam, ab31261, 1:500), rabbit anti-pAkt (phospho S473, Cell Signaling, 4060S, 1:100), and mouse anti-Rab7 (DSHB, Rab7, 1:100). Secondary antibodies used were goat anti-mouse 488 (Invitrogen, A11001, 1:250), donkey anti-rabbit 555 (Invitrogen, A31572, 1:250), goat anti-chicken 488 (Invitrogen, A11039, 1:250), and goat anti-mouse 633 (Invitrogen, A21050, 1:250).

Confocal Imaging. Brains were imaged on a Zeiss LSM 510 META laser scanning confocal microscope using 40X, 63X, and 100X oil immersion objectives (24). All collected images were projected in Zen software. Identical microscope setting was used to collect and analyze all genotypes for all trials within any given experiment. For three-dimensional (3D) images, the cropped Z-stack was processed with the 3D viewer icon in FIJI software to visualize PDF-Tri neurons, Repo-positive glia, and pAkt puncta. PDF-Tri neurons with glia colabeling Z-stacks were maximum projected in FIJI software to quantify the outlined neuronal area. Glial Rab5/7-labeled Z-stacks were sum projected to analyze total volumes. All Rab volumes were quantified only within labeled glia (*repo*-Gal4>mCD8::GFP membrane marker). The Rab volumes were divided by the imaged glial volume for normalization. The pAkt puncta within labeled PDF-Tri neurons were quantified based on 3D views. The number of pAkt puncta were divided by the PDF-Tri neuron area to quantify the pAkt puncta density.

Western Blots. Staged heads (3 to 5 h after eclosion at 25 °C) were homogenized in lysis buffer (20 mM HEPES, 10 mM EDTA, 100 mM KCl, 1% (v/v) Triton X-100, and 5% (v/v) glycerol, pH 7.4) with 2X protease and phosphatase inhibitor cocktail (Thermo Scientific, WL334851). Homogenized lysate samples (50 μL lysis buffer/head) were incubated on a rotor for 15 min at 4 °C and then centrifuged at 14,000 rpm for 15 min at 4 °C. The supernatant was denatured with 1X NuPAGE LDS sample buffer (Invitrogen, NP0007) for 10 min at 100 °C. Protein samples were run in 4 to 15% Mini-PROTEAN TGX gels (Bio-Rad, 4568086) and then transferred onto PVDF membranes using the Trans-Blot Turbo Transfer System (Bio-Rad). PVDF membranes were blocked in TBS Intercept Blocking Buffer (Li-COR# 220121) for 1 h at RT, followed by incubating with primary and secondary antibodies. Primary

antibodies used were rabbit anti-Smad3 (phospho S423+S425, Abcam, ab52903, 1:1,000), rabbit anti-pAkt (phospho S473, Cell Signaling, 4060S, 1:1,000), goat anti-GAPDH (glyceraldehyde 3-phosphate dehydrogenase) (Abcam, ab157156, 1:2,000), and chicken anti-APPL (a gift from Dr. Doris Kretzschmar, Oregon Health and Science University, USA; 1:1,000). Secondary antibodies used were goat anti-chicken 800 (Invitrogen, SA5-10076, 1:10,000), donkey anti-goat 680 (Invitrogen, A21084, 1:10,000), goat anti-mouse 800 (Invitrogen, SA535521, 1:10,000), and goat anti-rabbit 800 (Invitrogen, SA535571, 1:10,000). Blots were scanned with an Odyssey CLx Imager (Li-COR). Fluorescent band intensities were quantified using Image Studio Lite software (Li-COR). To normalize protein levels, the fluorescent intensity of targeted proteins was divided by the loading control of glyceraldehyde 3-phosphate dehydrogenase (GAPDH).

Quantitative Real-Time PCR. RNA was extracted for ~30 heads at 1 day posteclosion (1 dpe). The RNA extraction procedure followed the instructions of the RNeasy Plus Micro Kit (Qiagen, 74034). RNA (2 μg) was reversely transcribed in 20-μL reaction mixture of SuperScript VILO Master Mix (Invitrogen, 11755-050), with cDNA (1 μL) then mixed with 19 μL diluted *Power* SYBR Green PCR Master Mix (Applied Biosystems, 4367659) for real-time PCR amplification using the Bio-Rad CFX96 system. The quantified PCR cycle number was normalized to the internal control GAPDH. All primers used in this study are listed in *SI Appendix*, Table S2.

RNA Immunoprecipitation. The procedure was done as in Song et al. (24). Briefly; lysates were prepared from ~30 heads at 1 dpe with 500 μL RNase-free lysis buffer (20 mM HEPES, 100 mM NaCl, 2.5 mM EDTA, 0.05% (v/v) Triton X-100, 5% (v/v) glycerol, and 1% β-mercaptoethanol) with 1X protease inhibitor cocktail (cOmplete Mini EDTA-free tablets, Sigma-Aldrich) and 400 U RNase inhibitor (Applied Biosystems, N8080119). To precipitate RNA complexes, precleared lysates were incubated with 15 μL magnetic GFP-trap beads (ChromoTek) for 3 h at 4 °C, followed by washing 3X with lysis buffer. To purify bound RNAs, the washed beads were incubated with a 500 μL TRIzol and chloroform mixture (Ambion, 15596026) for 10 min. Subsequently, 1 μL glycogen was applied to carry RNAs for the precipitation by mixing with 100 μL 2-propenol. The above qPCR methods were performed to analyze the reverse-transcribed RNAs.

Statistical Analyses. All statistical analyses were performed with GraphPad Prism software 9.0. All datasets were subject to ROUT outlier tests with Q set to 1%. Unpaired two-tailed Student's *t* tests with 95% confidence of comparisons were used for all two-way datasets (PDF-Tri neuron areas, Rab7 volumes, pAkt puncta density, western blot assays, and qPCR assays). All datasets with more than two comparisons (day 1 and day 5 PDF-Tri neuron areas with *dfmr1* RNAi, *mad* RNAi, *prtp* RNAi, and *appl* RNAi) were analyzed by two-way ANOVA tests with a 5% alpha significance level. The comparison with more than two datasets was analyzed using one-way ANOVA tests (PDF-Tri neuron area). Data are presented as the mean ± SEM. Significance is indicated by *P* value measurements shown as $P < 0.05$ (*), $P < 0.01$ (**), $P < 0.001$ (***), and $P < 0.0001$ (****). Values of $P > 0.05$ are deemed not significant (ns).

Data, Materials, and Software Availability. All study data are included in this article and *SI Appendix*.

ACKNOWLEDGMENTS. We are particularly grateful to Dr. Benjamin Altenhein (University of Cologne, Germany) for the generous gift of the anti-Repo antibody and Dr. Doris Kretzschmar (Oregon Health and Science University, Portland, OR, USA) for the generous gift of the anti-APPL antibody. We thank the Bloomington *Drosophila* Stock Center (Indiana University, Bloomington, IN, USA) for essential genetic lines and the Developmental Studies Hybridoma Bank (University of Iowa, Iowa City, IA, USA) for essential antibodies. We are grateful to the Vanderbilt University Cell and Developmental Biology facility center and staff for help and the use of essential equipment. This work was entirely supported by funding from the National Institute of Mental Health R01 grant MH084989 to K.B.

Author affiliations: [a]Department of Biological Sciences, Vanderbilt University and Medical Center, Nashville, TN 37235; [b]Department of Cell and Developmental Biology, Vanderbilt University and Medical Center, Nashville, TN 37235; [c]Kennedy Center for Research on Human Development, Vanderbilt University and Medical Center, Nashville, TN 37235; and [d]Vanderbilt Brain Institute, Vanderbilt University and Medical Center, Nashville, TN 37235

1. A. Boulanger, J.-M. Dura, Neuron-glia crosstalk in neuronal remodeling and degeneration: Neuronal signals inducing glial cell phagocytic transformation in Drosophila. *Bioessays* **44**, 2100254 (2022).
2. S. Raiders *et al.*, Engulfed by Glia: Glial pruning in development, function, and injury across species. *J. Neurosci.* **41**, 823–833 (2021).
3. A. del Puerto, F. Wandosell, J. J. Garrido, Neuronal and glial purinergic receptors functions in neuron development and brain disease. *Front. Cell. Neurosci.* **7**, 197 (2013).
4. U. Neniskyte, C. T. Gross, Errant gardeners: Glial-cell-dependent synaptic pruning and neurodevelopmental disorders. *Nat. Rev. Neurosci.* **18**, 658–670 (2017).
5. E. Lee, W.-S. Chung, Glial control of synapse number in healthy and diseased brain. *Front. Cell. Neurosci.* **13**, 42 (2019).
6. O. J. Lieberman, A. F. McGuirt, G. Tang, D. Sulzer, Roles for neuronal and glial autophagy in synaptic pruning during development. *Neurobiol. Dis.* **122**, 49–63 (2019).
7. S. Marinelli, B. Basilico, M. C. Marrone, D. Ragozzino, Microglia-neuron crosstalk: Signaling mechanism and control of synaptic transmission. *Semin. Cell Dev. Biol.* **94**, 138–151 (2019).
8. J. A. Stogsdill, C. Eroglu, The interplay between neurons and glia in synapse development and plasticity. *Curr. Opin. Neurobiol.* **42**, 1–8 (2017).
9. R. D. Fields, D. H. Woo, P. J. Basser, Glial regulation of the neuronal connectome through local and long-distant communication. *Neuron* **86**, 374–386 (2015).
10. J. Juliani, N. Vassileff, J. G. Spiers, Inflammatory-mediated neuron-glia communication modulates ALS pathophysiology. *J. Neurosci.* **41**, 1142–1144 (2021).
11. A. Bernaus, S. Blanco, A. Sevilla, Glia crosstalk in neuroinflammatory diseases. *Front. Cell. Neurosci.* **14**, 209 (2020).
12. R. J. Hagerman *et al.*, Fragile X syndrome. *Nat. Rev. Dis. Primers* **3**, 1–19 (2017).
13. J. D. Richter, X. Zhao, The molecular biology of FMRP: New insights into fragile X syndrome. *Nat. Rev. Neurosci.* **22**, 209–222 (2021).
14. A. J. Verkerk *et al.*, Identification of a gene (FMR-1) containing a CGG repeat coincident with a breakpoint cluster region exhibiting length variation in fragile X syndrome. *Cell* **65**, 905–914 (1991).
15. C. L. Gatto, K. Broadie, Fragile X mental retardation protein is required for programmed cell death and clearance of developmentally-transient peptidergic neurons. *Dev. Biol.* **356**, 291–307 (2011).
16. S. H. Friedman, N. Dani, E. Rushton, K. Broadie, Fragile X mental retardation protein regulates trans-synaptic signaling in Drosophila. *Dis. Model Mech.* **6**, 1400–1413 (2013).
17. E. Donnard, H. Shu, M. Garber, Single cell transcriptomics reveals dysregulated cellular and molecular networks in a fragile X syndrome model. *PLoS Genet.* **18**, e1010221 (2022).
18. D. J. Vita, C. J. Meier, K. Broadie, Neuronal fragile X mental retardation protein activates glial insulin receptor mediated PDF-Tri neuron developmental clearance. *Nat. Commun.* **12**, 1160 (2021).
19. C. Song, K. Broadie, Dysregulation of BMP, Wnt, and insulin signaling in Fragile X syndrome. *Front. Cell Dev. Biol.* **10**, 934662 (2022).
20. L. Deignan *et al.*, Regulation of the BMP signaling-responsive transcriptional network in the Drosophila embryo. *PLoS Genet.* **12**, e1006164 (2016).
21. E. J. Gallagher, D. LeRoith, "Insulin mechanisms/metabolic actions" in *Encyclopedia of Biological Chemistry*, W. J. Lennarz, M. D. Lane, Eds. (Academic Press, ed. 2, 2013), pp. 602–607.
22. J. J. L. Wong *et al.*, A Cullin1-based SCF E3 ubiquitin ligase targets the InR/PI3K/TOR pathway to regulate neuronal pruning. *PLoS Biol.* **11**, e1001657 (2013).
23. M. Ascano *et al.*, FMRP targets distinct mRNA sequence elements to regulate protein expression. *Nature* **492**, 382–386 (2012).
24. C. Song, S. N. Leahy, E. M. Rushton, K. Broadie, RNA-binding FMRP and Staufen sequentially regulate the coracle scaffold to control synaptic glutamate receptor and bouton development. *Development* **149**, dev200045 (2022).
25. B. Bu, L. Zhang, A new link between insulin signaling and Fragile X syndrome. *Neurosci. Bull.* **33**, 118–120 (2017).
26. T. Kuraishi *et al.*, Pretaporter, a Drosophila protein serving as a ligand for Draper in the phagocytosis of apoptotic cells. *EMBO J.* **28**, 3868–3878 (2009).
27. I. A. Kessissoglou *et al.*, The Drosophila amyloid precursor protein homologue mediates neuronal survival and neuroglial interactions. *PLoS Biol.* **18**, e3000703 (2020).
28. R. Nakano *et al.*, Cortex glia clear dead young neurons via Drpr/dCed-6/Shark and Crk/Mbc/dCed-12 signaling pathways in the developing Drosophila optic lobe. *Dev. Biol.* **453**, 68–85 (2019).
29. C. Gross, G. J. Bassell, Excess protein synthesis in FXS patient lymphoblastoid cells can be rescued with a P110β-selective inhibitor. *Mol. Med.* **18**, 336–345 (2012).
30. A. R. Armstrong, D. Drummond-Barbosa, Insulin signaling acts in adult adipocytes via GSK-3β and independently of FOXO to control Drosophila female germline stem cell numbers. *Dev. Biol.* **440**, 31–39 (2018).
31. J. Gil-Ranedo *et al.*, STRIPAK members orchestrate hippo and insulin receptor signaling to promote neural stem cell reactivation. *Cell Rep.* **27**, 2921–2933.e5 (2019).
32. C. J. Westmark, J. S. Malter, FMRP mediates mGluR5-dependent translation of amyloid precursor protein. *PLoS Biol.* **5**, e52 (2007).
33. C. J. Westmark *et al.*, APP causes hyperexcitability in fragile X mice. *Front. Mol. Neurosci.* **9**, 147 (2016).
34. J. Folch *et al.*, The implication of the brain insulin receptor in late onset Alzheimer's disease dementia. *Pharmaceuticals.* **11**, 11 (2018).
35. E. Kurant, S. Axelrod, D. Leaman, U. Gaul, Six-microns-under acts upstream of draper in the glial phagocytosis of apoptotic neurons. *Cell* **133**, 498–509 (2008).
36. E. C. Damisah *et al.*, Astrocytes and microglia play orchestrated roles and respect phagocytic territories during neuronal corpse removal in vivo. *Sci. Adv.* **6**, eaba3239 (2020).
37. F. M. Skjeldal *et al.*, De novo formation of early endosomes during Rab5-to-Rab7a transition. *J. Cell Sci.* **134**, jcs254185 (2021).
38. H. Shu *et al.*, FMRP links optimal codons to mRNA stability in neurons. *Proc. Natl. Acad. Sci. U.S.A.* **117**, 30400–30411 (2020).
39. F. Zhang *et al.*, Fragile X mental retardation protein modulates the stability of its m6A-marked messenger RNA targets. *Hum. Mol. Genet.* **27**, 3936–3950 (2018).
40. H. Urrutia, A. Aleman, E. Eivers, Drosophila dullard functions as a mad phosphatase to terminate BMP signaling. *Sci. Rep.* **6**, 32269 (2016).
41. J. Sardi *et al.*, Mad dephosphorylation at the nuclear pore is essential for asymmetric stem cell division. *Proc. Natl. Acad. Sci. U.S.A.* **118**, e2006786118 (2021).

42. I. V. Saltykova *et al.*, Tribbles homolog 3-mediated targeting the AKT/mTOR axis in mice with retinal degeneration. *Cell Death Dis.* **12**, 1–11 (2021).
43. T. P. Das, S. Suman, H. Alatassi, M. K. Ankem, C. Damodaran, Inhibition of AKT promotes FOXO3a-dependent apoptosis in prostate cancer. *Cell Death Dis.* **7**, e2111 (2016).
44. H. J. Jung, Y. Suh, Regulation of IGF-1 signaling by microRNAs. *Front. Genet.* **5**, 472 (2015).
45. A. Dutriaux, A. Godart, A. Brachet, J. Silber, The insulin receptor is required for the development of the Drosophila peripheral nervous system. *PLoS One* **8**, e71857 (2013).
46. Y. Fuchs, H. Steller, Programmed cell death in animal development and disease. *Cell* **147**, 742–758 (2011).
47. R. B. Birge, D. S. Ucker, Innate apoptotic immunity: The calming touch of death. *Cell Death Differ.* **15**, 1096–1102 (2008).
48. M. Riera Romo, Cell death as part of innate immunity: Cause or consequence? *Immunology* **163**, 399–415 (2021).
49. C. N. McLaughlin, J. J. Perry-Richardson, J. C. Coutinho-Budd, H. T. Broihier, Dying neurons utilize innate immune signaling to prime glia for phagocytosis during development. *Dev. Cell* **48**, 506–522.e6 (2019).
50. S. Xu, J. Lu, A. Shao, J. H. Zhang, J. Zhang, Glial cells: Role of the immune response in ischemic stroke. *Front. Immunol.* **11**, 294 (2020).
51. Y.-B. Hu, E. B. Dammer, R.-J. Ren, G. Wang, The endosomal-lysosomal system: From acidification and cargo sorting to neurodegeneration. *Transl. Neurodegener.* **4**, 18 (2015).
52. G. G. Vandenberg, N. J. Dawson, A. Head, G. R. Scott, A. L. Scott, Astrocyte-mediated disruption of ROS homeostasis in Fragile X mouse model. *Neurochem. Int.* **146**, 105036 (2021).
53. T. Gu, T. Zhao, R. S. Hewes, Insulin signaling regulates neurite growth during metamorphic neuronal remodeling. *Biol. Open* **3**, 81–93 (2013).
54. D. T. Musashe, M. D. Purice, S. D. Speese, J. Doherty, M. A. Logan, Insulin-like signaling promotes glial phagocytic clearance of degenerating axons through regulation of draper. *Cell Rep.* **16**, 1838–1850 (2016).
55. N. J. Harrison *et al.*, Regenerative neurogenic response from glia requires insulin-driven neuron-glia communication. *Elife* **10**, e58756 (2021), 10.7554/eLife.58756.
56. Q. Dong *et al.*, Glial Hedgehog signalling and lipid metabolism regulate neural stem cell proliferation in Drosophila. *EMBO Rep.* **22**, e52130 (2021).